Supporting Information

Carbon- and Crack-free Growth of Hexagonal Boron Nitride Nanosheets and Their Uncommon Stacking Order

Majharul Haque Khan[a,b], Gilberto Casillas[c], David R.G. Mitchell[c], Hua Kun Liu[b], Lei Jiang[d], Zhenguo Huang[a,b,*]

[a]Key Laboratory of Electromagnetic Processing of Materials (Ministry of Education), Northeastern University, Shenyang, 110819, China.
[b]Institute for Superconducting and Electronic Materials, University of Wollongong, Wollongong, NSW 2500, Australia
[c]Electron Microscopy Centre, University of Wollongong, Wollongong, NSW 2500, Australia
[d]Beijing National Laboratory of Molecular Sciences (BNLMS), Key Laboratory of Organic Solid, Institute of Chemistry, Chinese Academy of Sciences, Beijing, PR China

*Corresponding author: zhenguo@uow.edu.au

Results and Discussion:

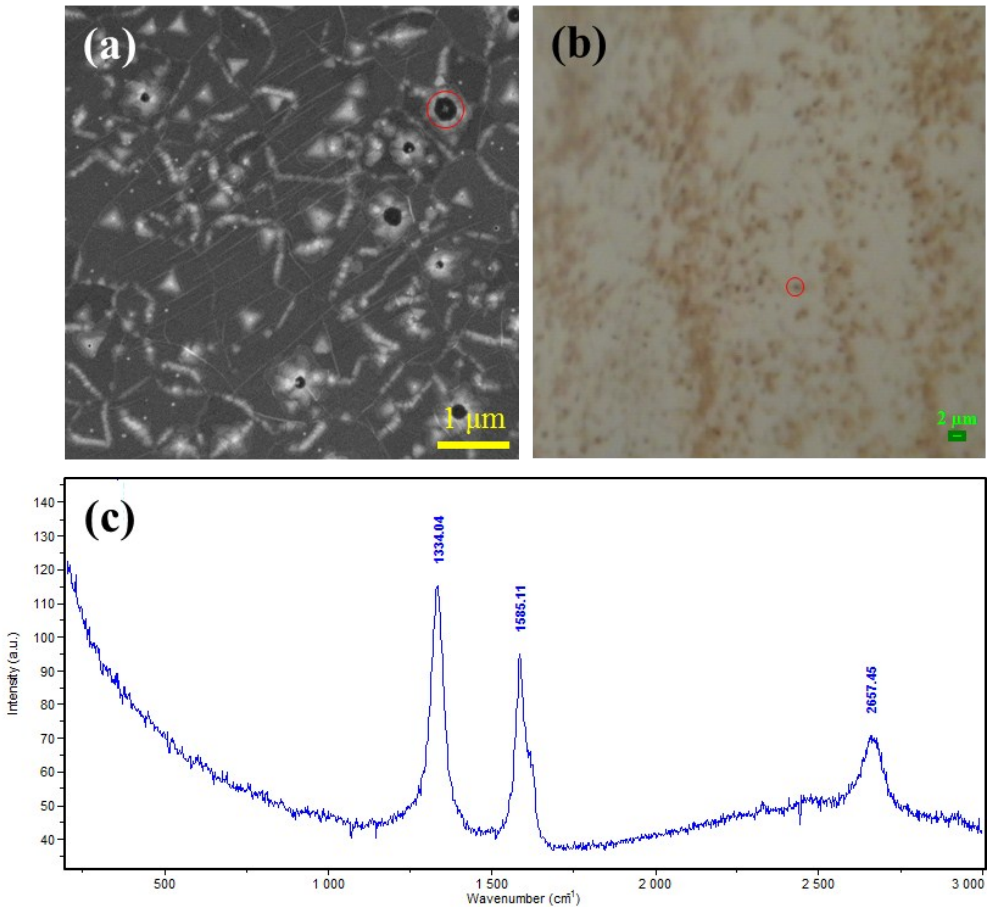

Figure S1. Carbon contamination due to residual solvents in the ammonia borane precursor. (a) Using the as-received ammonia borane leads to graphite-like structure on top of *h*-BNNS, which appears as dark spots in SEM images. (b) Optical image of the sample. (c) Raman spectrum from the circled spots in (a) and (b) shows the I_D (1334.04 cm^{-1}), I_G (1585.11 cm^{-1}), and I_{2D} (2657.45 cm^{-1}) peaks of graphite.

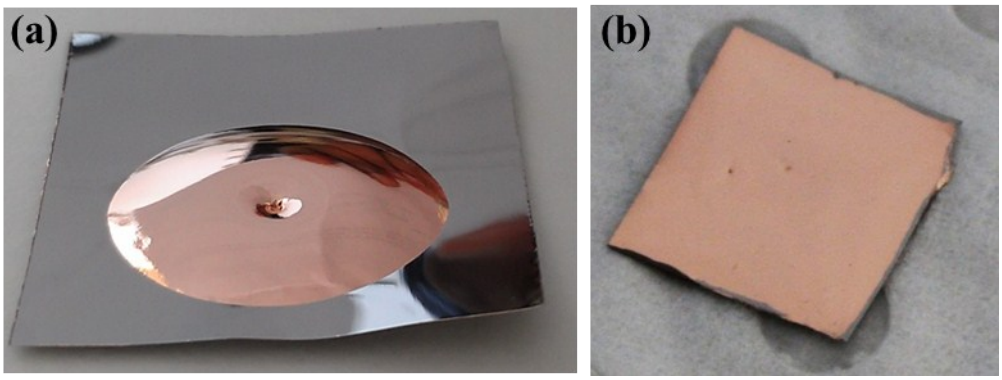

Figure S2. Images of Cu foils on W after 1100 °C melting and then solidification. (a) Without flattening the Cu and W foils, an elliptical-shaped Cu surface is formed on the W while (b) flattening the foils can produce a uniform wetted Cu surface.

(a)

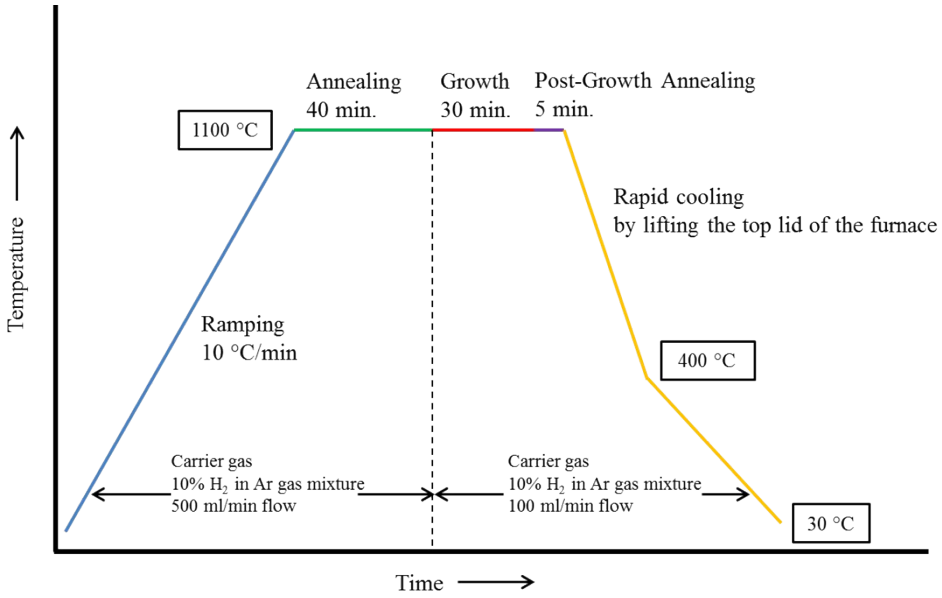

(b)

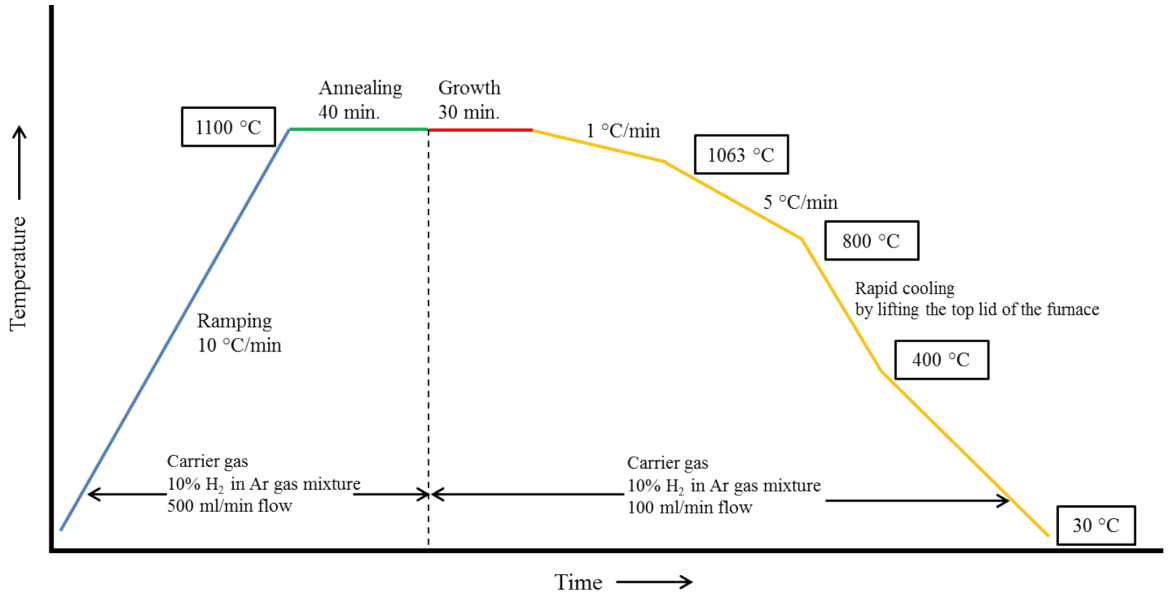

Figure S3. Time-temperature profiles for the CVD growth of *h*-BNNS. (a) Fast cooling process and (b) slow cooling process after the growth, while all the other parameters were kept fixed.

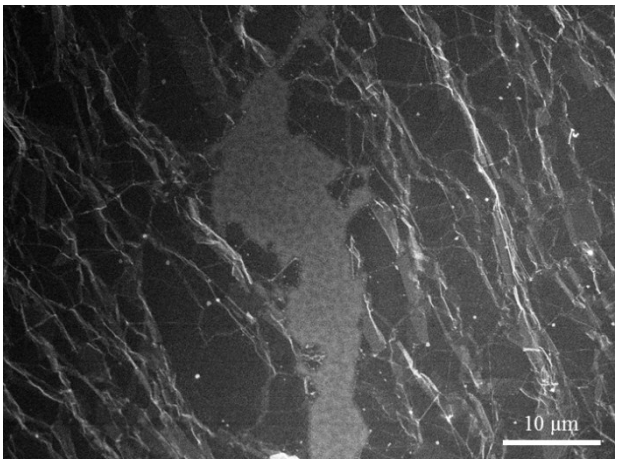

Figure S4. When the Cu and W foils were not flattened prior to the growth, cracks generated around the centre of an elliptically shaped Cu surface cannot be avoided, even with a slow cooling through the Cu melting point.

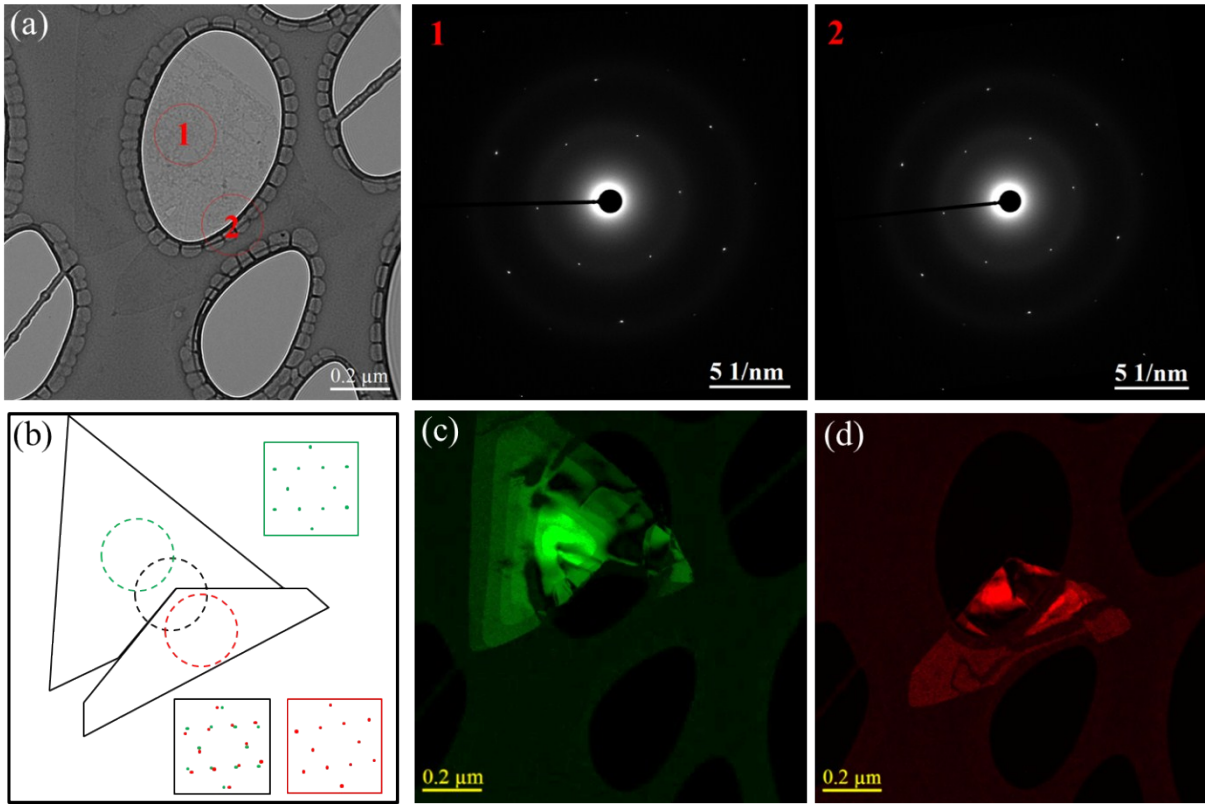

Figure S5. (a) Bright-field (BF) – TEM image of two merged triangular *h*-BNNS crystals. Selected area electron diffraction (SAED) patterns obtained from the individual triangles (marked 1 and 2 in (a)) demonstrate the single crystal nature of each triangular particle. There is about an 8° rotational orientation difference between these two crystals (main manuscript, Figure 4b). (b) Schematic diagram of the overlapping triangular crystals and the corresponding SAED patterns. (c) and (d) Dark-field (DF)-TEM images acquired using the red and green aperture locations, respectively, indicated in Figure 4b in the main text.

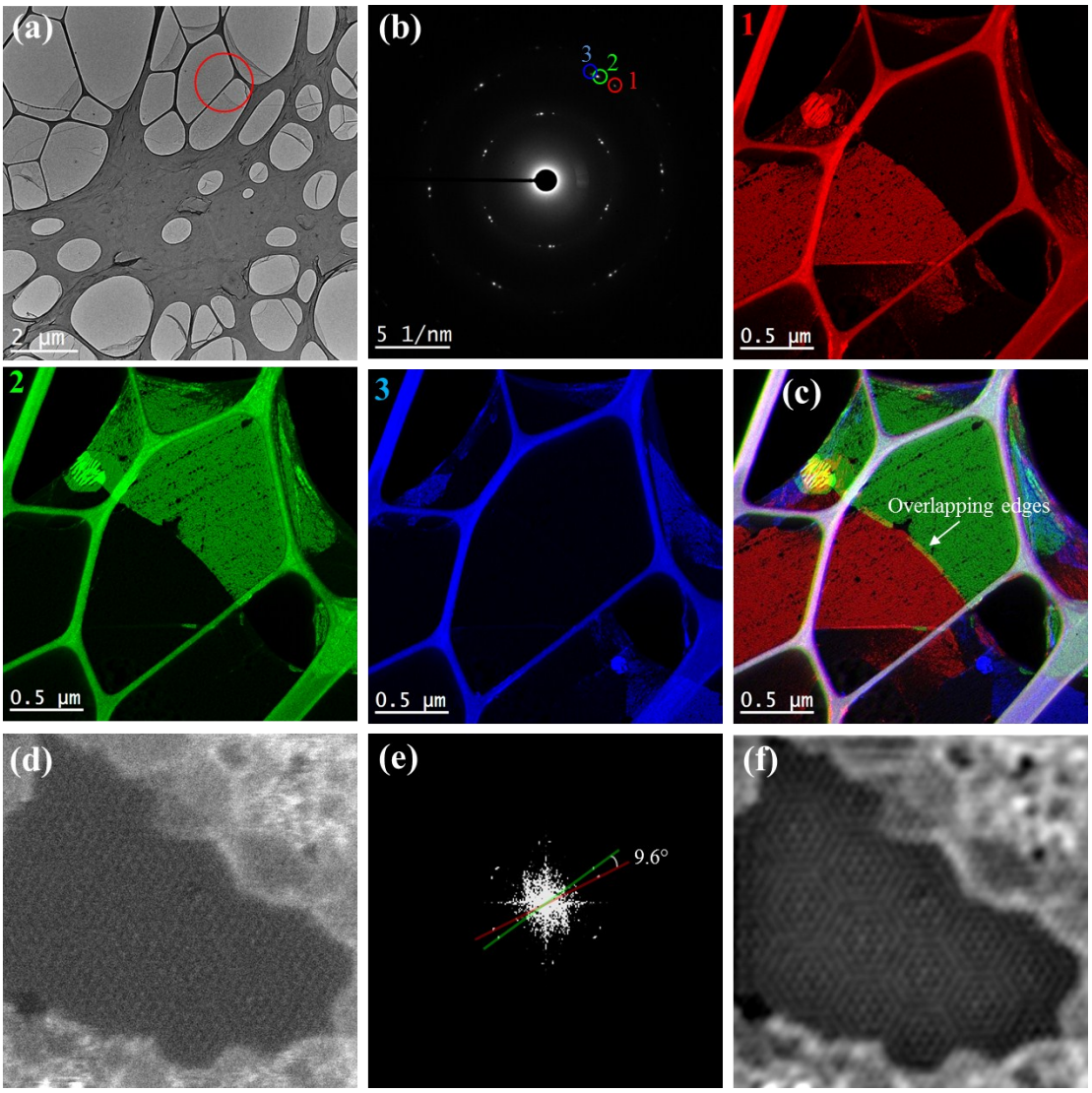

Figure S6. (a) TEM image of *h*-BNNS on a lacey carbon TEM grid. (b) SAED pattern taken from the red-circle in (a) reveals three differently oriented *h*-BN crystals in that region. (1), (2), and (3) DF-TEM images obtained using the red, green, and blue objective aperture positions marked in (b) (numbered 1, 2, and 3, respectively). The DF-TEM images have been coloured according to the aperture filter and colour, as shown in (b). (c) A combined DF-TEM image reveals the crystalline structure in each region. Overlapping of the edges is revealed by the different colour contrast (yellow colour from the mixing of the red and green colours, according to the RGB colour model (shown in the inset of Figure 4(e)). Therefore, no definite grain boundaries are seen in the *h*-BNNS grown on melted Cu substrate. (d) Raw annular dark-field (ADF)-STEM image from the overlapped region shown in (c). (e) Fast Fourier transform (FFT) pattern obtained from (d), showing two different sets of hexagonal spots, rotated about 9.6° with respect to each other. (f) FFT filtered image of (d) showing a clear Moiré pattern developed due to the absence of definite stacking orders.

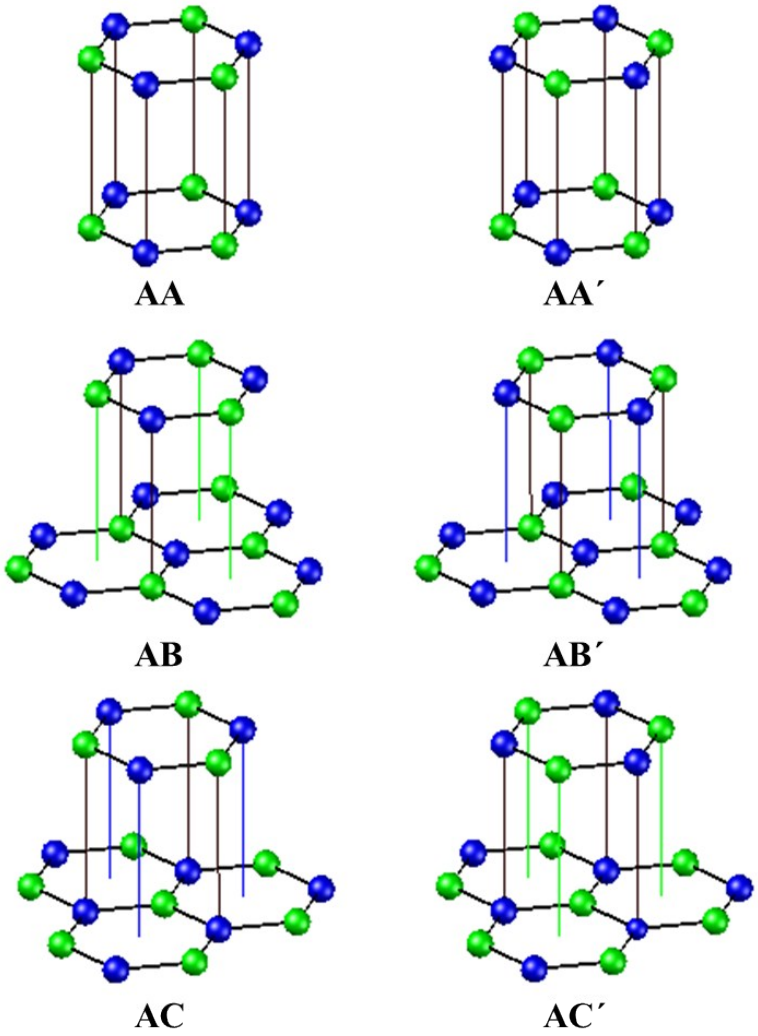

Figure S7. Illustration of six different types of bi-layer stacking for *h*-BN. The green and blue spheres represent boron and nitrogen atoms, respectively.

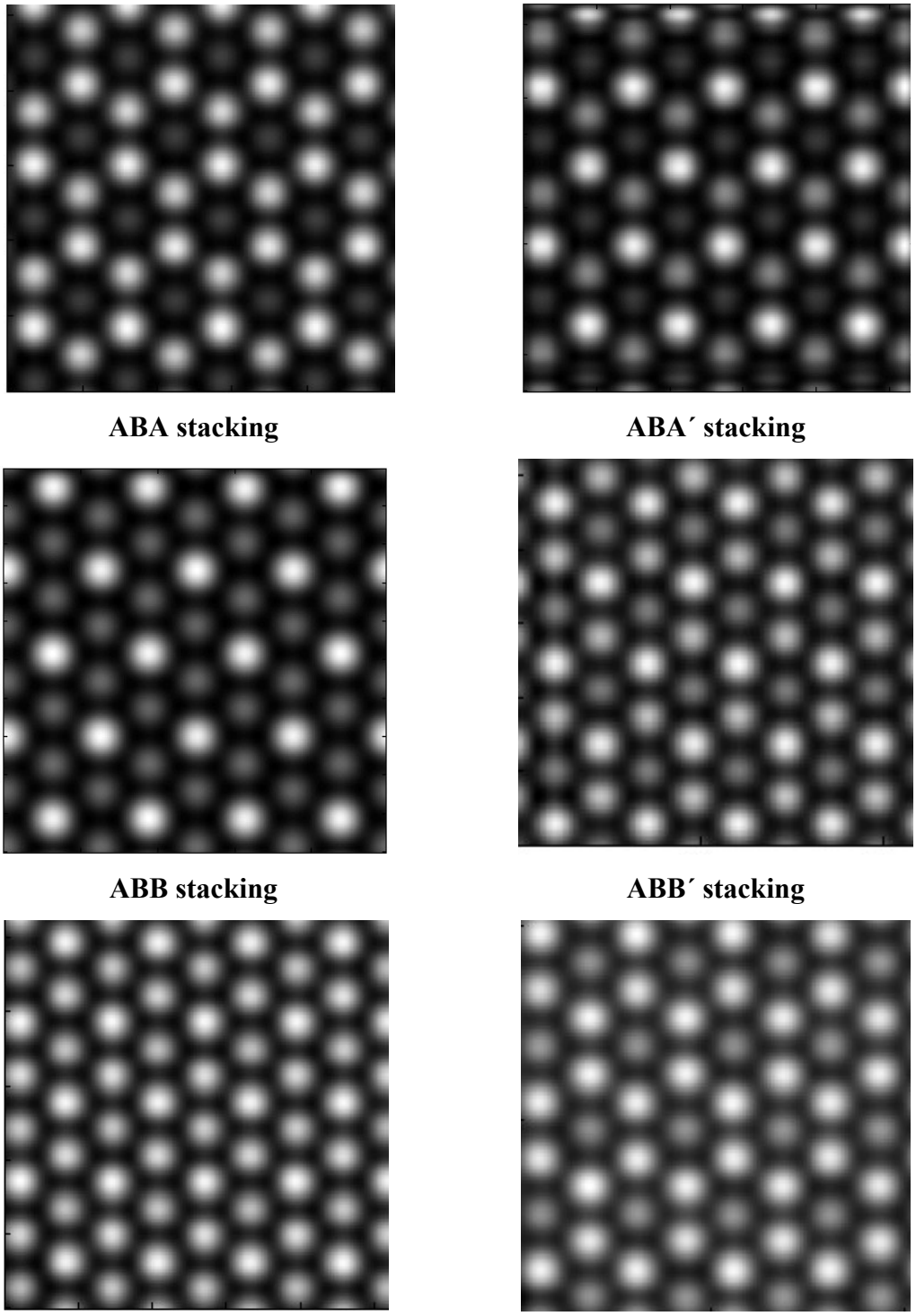

Figure S8. Simulated annular dark-field (ADF)-STEM images of the six different types of *h*-BN stacking possible for the three-layered film in Figure 5b. The first two layers of this three-layered structure have been found to be AB (Figure 5a). Therefore, 6 other stacking orders are possible in the third layer.